The EMBO Journal (2004) 23, 3909–3917 | © 2004 European Molecular Biology Organization | All Rights Reserved 0261-4189/04
www.embojournal.org

THE EMBO JOURNAL

Crystal structure of human GGA1 GAT domain complexed with the GAT-binding domain of Rabaptin5

Guangyu Zhu[1,4], Peng Zhai[1,4], Xiangyuan He[2], Nancy Wakeham[1], Karla Rodgers[3], Guangpu Li[3], Jordan Tang[2,3] and Xuejun C Zhang[1,*]

[1]Crystallography Research Program, Oklahoma Medical Research Foundation, Oklahoma City, OK, USA, [2]Protein Studies Program, Oklahoma Medical Research Foundation, Oklahoma City, OK, USA and [3]Department of Biochemistry and Molecular Biology, University of Oklahoma Health Sciences Center, Oklahoma City, OK, USA

GGA proteins coordinate the intracellular trafficking of clathrin-coated vesicles through their interaction with several other proteins. The GAT domain of GGA proteins interacts with ARF, ubiquitin, and Rabaptin5. The GGA–Rabaptin5 interaction is believed to function in the fusion of *trans*-Golgi-derived vesicles to endosomes. We determined the crystal structure of a human GGA1 GAT domain fragment in complex with the Rabaptin5 GAT-binding domain. In this structure, the Rabaptin5 domain is a 90-residue-long helix. At the N-terminal end, it forms a parallel coiled-coil homodimer, which binds one GAT domain of GGA1. In the C-terminal region, it further assembles into a four-helix bundle tetramer. The Rabaptin5-binding motif of the GGA1 GAT domain consists of a three-helix bundle. Thus, the binding between Rabaptin5 and GGA1 GAT domain is based on a helix bundle–helix bundle interaction. The current structural observation is consistent with previously reported mutagenesis data, and its biological relevance is further confirmed by new mutagenesis studies and affinity analysis. The four-helix bundle structure of Rabaptin5 suggests a functional role in tethering organelles.

The EMBO Journal (2004) **23,** 3909–3917. doi:10.1038/sj.emboj.7600411; Published online 30 September 2004
Subject Categories: structural biology; membranes & transport
Keywords: crystal structure; GAT domain; GGA proteins; intracellular trafficking; Rabaptin5

Introduction

Clathrin-coated vesicles (CCVs) represent a major type of vesicular carrier that traffics between *trans*-Golgi network (TGN) and endosomes, as in the case of lysosomal enzyme transport, and from the plasma membrane to early endosomes, as in the case of receptor-mediated endocytosis (Kirchhausen, 2000). The clathrin lattice interacts with membrane or membrane-bound proteins through adaptor proteins. The GGA family of adaptor proteins (Golgi-localized, γ-ear-containing, and ARF-binding) plays important roles in the CCV trafficking between TGN and endosome compartments (Boman *et al*, 2000; Dell'Angelica *et al*, 2000; Hirst *et al*, 2000; Poussu *et al*, 2000) and probably also in endocytosis (Puertollano and Bonifacino, 2004), including cargo selection and recruitment of clathrin and accessory proteins to the budding site. GGAs are monomeric proteins present in a variety of organisms. There are three isoforms, GGA1–3, in higher eukaryotic cells. The cellular function of GGA proteins in vesicular trafficking is manifested largely through the interactions of its four domains with other protein partners. In the order of N- to C-terminus, the four domains are VHS (VPS27, Hrs, and STAM homologous), GAT (GGA and TOM1 homologous), hinge region, and GAE (γ-adaptin ear homologous) (Dell'Angelica *et al*, 2000; Hirst *et al*, 2000; Takatsu *et al*, 2000, 2002; Puertollano *et al*, 2001). The GAT domain has been shown to interact with the membrane-bound form of ARF, a GTPase molecular switch initiating CCV assembly (Moss and Vaughan, 1998). The interaction between GAT domain and ARF (Dell'Angelica *et al*, 2000; Boman, 2001; Takatsu *et al*, 2002) defines the vesicle-assembling site on the membrane and facilitates subsequent interactions with other proteins in the assembly complex (Dell'Angelica *et al*, 2000). Recently, the GAT domain is shown to interact with Rabaptin5 and ubiquitin using overlapped binding sites (Zhai *et al*, 2003; Mattera *et al*, 2004; Shiba *et al*, 2004). The GAE domain has an immunoglobulin fold and interacts with an array of accessory ligands, including an extended peptide strand from Rabaptin5 (Hirst *et al*, 2000; Takatsu *et al*, 2000; Miller *et al*, 2003). Since the GAT domain also interacts with Rabaptin5, the interaction between GGA and Rabaptin5 is divalent in nature. The structure of GGA1 GAT domain comprises four helices in an overall elongated shape, in which the longest helix participates in two structural motifs: an N-terminal helix–loop–helix motif and a C-terminal three-helix bundle (Collins *et al*, 2003; Shiba *et al*, 2003; Suer *et al*, 2003; Zhu *et al*, 2003). The N-terminal motif contains a hydrophobic surface patch, which is found to interact directly with ARF in a crystal structure (Shiba *et al*, 2003). The C-terminal three-helix bundle is involved in the binding with Rabaptin5 (Zhai *et al*, 2003; Mattera *et al*, 2004) and ubiquitin (Scott *et al*, 2004; Shiba *et al*, 2004).

Rabaptin5, a 99-kDa protein, was initially identified as an effector of Rab5 in the fusion of early endosomes (Stenmark *et al*, 1995). The involvement of Rabaptin5 in this process is an essential and rate-limiting step. While located mainly in the cytosol, Rabaptin5 is also present at low levels on the cell membrane (Gournier *et al*, 1998). Secondary structure prediction from the amino-acid sequence suggests that

*Corresponding author. Crystallography Research Program, Oklahoma Medical Research Foundation, 825 NE 13th Street, Oklahoma City, OK 73104, USA. Tel.: +1 405 271 7402; Fax: +1 405 271 7953; E-mail: zhangc@omrf.ouhsc.edu
[4]These authors contributed equally to this work

Received: 21 June 2004; accepted: 19 August 2004; published online: 30 September 2004

Rabaptin5 contains multiple coiled-coil regions, each of which is capable of forming homodimers *in vitro* (Stenmark *et al*, 1995). It has been shown that one of the predicted coiled-coil regions in human Rabaptin5, consisting of residues 551–661, binds the GAT domain of GGA1 and GGA2 (Mattera *et al*, 2003). Besides GGAs, Rabaptin5 divalently interacts with the γ-adaptin subunit of AP-1 complex (Shiba *et al*, 2002; Mattera *et al*, 2003), which is a major component of the CCV coating complex at the TGN. Rabaptin5 is also involved in the endosome-recycling pathway through its interaction with Rab4 (Vitale *et al*, 1998). Members of the Rabaptin5 family from different species are highly homologous in their primary sequences. In human cells, there exist a number of Rabaptin5 splicing variants (Korobko *et al*, 2002; Deneka *et al*, 2003), but their functional roles are yet to be determined. Among these splicing variants, there is no deletion/insertion observed around the GAT-binding region.

While it is known that a short peptide motif in Rabaptin5 is responsible for interacting with the GAE domain of GGAs, the structural motif of Rabaptin5 mediating the GAT binding remains to be identified. Here, we present the crystal structure of the three-helix bundle motif of human GGA1 GAT domain in complex with the GAT-binding domain of Rabaptin5. The GAT–Rabaptin5 interaction has a helix bundle–helix bundle-binding mode, in which one GAT domain binds to a pseudo-symmetric Rabaptin5 dimer. Furthermore, a four-helix bundle formation is observed for the Rabaptin5$^{551–661}$ fragment in both crystal and solution, suggesting a direct functional role of Rabaptin5 in tethering organelles.

Results

Overall structure of the GAT–Rabaptin5 complex

To determine the complex structure of GGA1 GAT and Rabaptin5 fragments, we expressed and purified recombinant proteins of GGA1$^{210–302}$ (i.e. residues 210–302 of GGA1, the three-helix bundle motif of the GAT domain) and Rabaptin5$^{551–661}$ (Figure 1A) from *Escherichia coli* and cocrystallized them. The crystal form belongs to $P3_221$ space group with one GGA1$^{210–302}$ and two Rabaptin5$^{551–661}$ molecules per asymmetric unit (asu) (Table I, Figure 1B). The molecular surface of this GAT–Rabaptin5$_2$ complex is dominated by negatively charged electrostatic potential (Figure 1C), consistent with the calculated pI values of 4.7 and 5.2 for the GGA1$^{210–302}$ and Rabaptin5$^{551–661}$ recombinant proteins, respectively. The structure of the three-helix bundle (i.e. helices α_2–α_4) of GAT is essentially the same as that from the full-length GAT (Protein Data Bank (PDB) file 1OXZ) (Zhu *et al*, 2003), with a C_α-atom root mean square deviation (r.m.s.d.) of 0.92 Å between them. The Rabaptin5-binding site has an even better agreement between the two structures (a 0.47 Å C_α-r.m.s.d. for residues 257–270 and 274–288). A few regions of high mobility in GGA1$^{210–302}$, including the connecting loop between helices α_2 and α_3 and a couple of residues from both termini, are omitted from the final refined model. Similarly omitted are mobile residues in Rabaptin5$^{551–661}$ that are either at the N-terminus or C-terminal to Glu640^R (the superscript R stands for Rabaptin5). Each of the two Rabaptin5$^{551–661}$ chains contains one long helix of 24 turns (~90 residues) with an overall length of 135 Å. The two Rabaptin5 chains in one asu form a parallel coiled-coil homodimer at their N-terminal region, which binds to helices

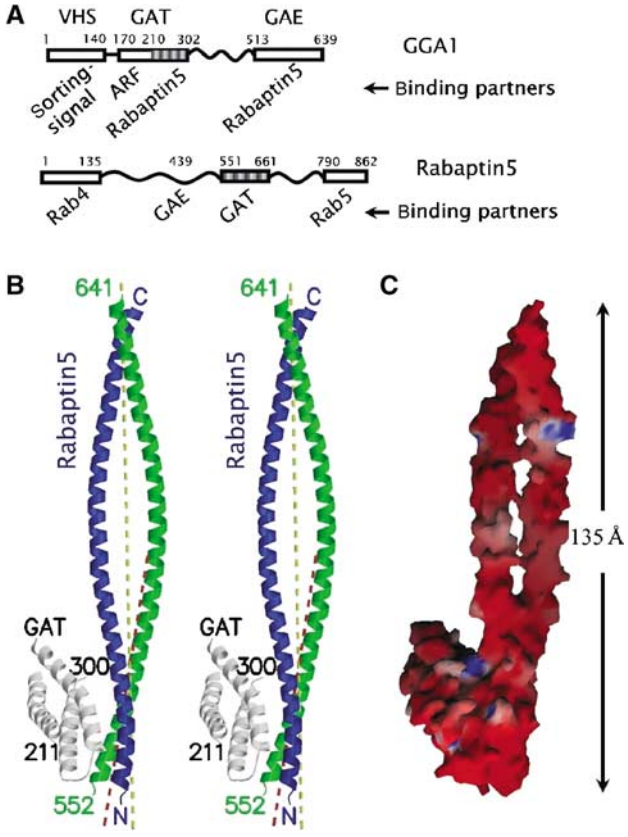

Figure 1 GAT–Rabaptin5 complex. (**A**) Schematic diagram of the constructs of GAT and Rabatin5 fragments. Known domains are shown as boxes with the residue numbers and names (if existing) marked on top. Relevant binding partners are listed below. Regions included in the crystal are shaded. (**B**) Stereo view of a ribbon diagram of the complex of GGA1 GAT three-helix bundle domain (white) and Rabaptin5$^{551–661}$ (blue and green). The crystallographically visible peptide termini are labeled either as N/C or with residue numbers. The major local two-fold axis of the Rabaptin5$^{551–661}$ homodimer is depicted as a yellow dash line, and the two-fold axis of the GAT-binding region is shown as a red dash line. (**C**) Molecular surface model of the complex. The color intensity corresponds to the electrostatic potential calculated with the program *GRASP* and its default parameters, from $-8\,kTe^{-1}$ (intense red) to $+8\,kTe^{-1}$ (intense blue). Figures 1B, 2A, 4A, and 6 were drawn with the programs *MolScript* and *Raster3D*. Figures 1C and 2B were drawn with the program *GRASP*.

α_3 and α_4 of the three-helix bundle of GGA1$^{210–302}$. The helix–helix distance (9.3 Å) and crossing angle (20°) in this Rabaptin5 N-terminal region are typical for a coiled-coil dimer (Lupas, 1996). Furthermore, this homodimer region bends by about 10° from the dyad axis of the remaining homodimer (Figure 1B), where the helix–helix distance and crossing angle become 13.5 Å and 28°, respectively (calculated from residues 611–620). The bending of the Rabaptin5 dimer in the GAT-binding region toward its ligand could be an artifact of crystallization, but it is more likely that the bending is induced by the intimate interaction with GAT. Thus, the conformations of two Rabaptin5$^{551–661}$ chains in one asu (i.e. the green and blue chains in Figure 1B) are similar but not identical to each other. Their overall C_α-r.m.s.d. is 2.3 Å, as compared to that of 0.93 Å for the N-terminal coiled-coil homodimer (i.e. residues 555–576) alone and 0.75 Å for the rest of the long helix. Furthermore, we found unexpectedly

Table I Statistics of crystallographic data, phasing, and refinement

Data collection					
Space group	$P3_221$				
Cell dimensions	$a=b=155.2$ Å, $c=53.1$ Å				
			Se-Met		
	Native	λ_1 (remote)	λ_2 (peak)	λ_3 (inf.)	
Wavelength used (Å)	1.5418	0.95667	0.97938	0.97952	
Resolution range (Å)	50 (2.49)[a]–2.40	20 (2.90)–2.80	20 (2.90)–2.80	20 (2.90)–2.80	
No. of measurements	148 886	126 001	122 613	122 550	
No. of unique reflections	28 214 (2217)	18 160	18 008	17 972	
Completeness (%)	97.2 (77.3)	98.6 (99.5)	98.0 (95.6)	97.9 (95.6)	
$I/\sigma(I)$	30.1 (2.3)	19.2 (4.3)	20.6 (4.7)	20.6 (4.9)	
R_{merge}[b] (%)	5.4 (40.5)	8.7 (39.8)	8.3 (34.2)	8.0 (33.1)	
Phase power[c] *and figure of merit (FOM)*		*Observed diffraction ratios*[d]			
Resolutions (Å)	20(2.92)–2.79		λ_1	λ_2	λ_3
Phase power		λ_1	0.085	0.082	0.105
λ_1–λ_1^-	0.91 (0.55)	λ_2		0.077	0.096
λ_1–λ_2^+	0.80 (0.58)	λ_3			0.088
λ_1–λ_2^-	1.32 (0.68)				
λ_1–λ_3^+	1.04 (0.51)				
λ_1–λ_3^-	1.38 (0.69)				
FOM	0.50 (0.28)				
Refinement					
Resolution (Å)	55–2.4				
$R_{working}$[e] (%)/no. of reflections	23.3/22 743				
R_{free}[e] (%)/no. of reflections	28.3/910				
No. of non-hydrogen atoms	2246				
R.m.s.d. from ideal values					
Bond length (Å)	0.013				
Bond angle (deg)	1.4				
Improper angle (deg)	0.91				
Dihedral angle (deg)	16.9				
Average *B*-factor (Å^2)	58.3 (45.9)[f]				

[a]Values in parentheses are for the highest resolution bin.
[b]$R_{merge}=\sum_h\sum_i|I_i(h)-I(h)\rangle|/\sum_h\sum_i I_i(h)$, where $I_i(h)$ is the ith measurement and $\langle I(h)\rangle$ is the mean of all measurements of $I(h)$ for Miller indices h.
[c]MAD phasing power is defined as $(\langle|F_D-F_N|^2\rangle/\int\varphi P(\varphi)(|F_N\exp(i\varphi)+\Delta F_H|-F_D)^2\,d\varphi)^{1/2}$, where $P(\varphi)$ is the experimental phase probability distribution, F_N is the amplitude of the structure factor at the reference wavelength λ_1, F_D corresponds to the structure factor at wavelength λ_i (indicated by the superscript '+') or its *Friedel* mate (indicated by the superscript '−'), and ΔF_H is the difference in heavy atom structure factors between the two wavelengths. Similarly, the phasing power of a derivative is defined between the derivative and native data.
[d]Values are $\langle(\Delta F)^2\rangle^{1/2}/\langle F^2\rangle^{1/2}$, where ΔF is the dispersive (off-diagonal elements) or *Bijvoet* difference (diagonal elements), computed between 30 and 2.8 Å resolution.
[e]$R=\sum(F_{obs}-kF_{calc})/\sum F_{obs}$; all reflections of $F>0$ in the resolution range were included.
[f]Wilson thermal factor of the native dataset.

in the crystal that two crystallographic symmetry-related Rabaptin5 dimers form a homotetramer using their C-terminal helical fragments, which is organized into a left-hand twisted four-helix bundle (see below).

GAT–Rabaptin5 interaction

The N-terminal homodimer and the C-terminal four-helix bundle regions of Rabaptin5$^{551–661}$ have individual local symmetries. However, only one GGA1$^{210–302}$ domain binds with the N-terminal symmetric homodimer, although it interacts with both monomers. The solvent-accessible surface (SAS) buried upon complex formation between one GAT molecule and Rabaptin5 homodimer is 1770 Å^2, with 52% from hydrophobic atoms. The only other interaction between GAT and Rabaptin5 observed in the crystal packing is significantly smaller, with buried SAS less than 600 Å^2. It unlikely bears any biological function.

In the crystal structure, the Rabaptin5-binding residues from GGA1$^{210–302}$ form a central hydrophobic strip that is surrounded by charged or polar residues (Figure 2 and Supplementary Figure S1). The interacting residues in Rabaptin5$^{551–661}$ include Gln556^R, Lys559^R, Met563^R, Gln566^R, and Lys573^R from one monomer, and Arg554^R, Gln561^R, Leu564^R, Arg565^R, Asn568^R, and Met575^R from the other. They also form a hydrophobic strip in the center of the binding patch (Figure 2B). The interaction between the two proteins is extensive and fairly complimentary. For example, a surface socket formed by residues Phe264, Ser268, Leu277, and Leu281 of GGA1 is complementary with the side chain of Met563^R. Similarly, the GGA1 Phe264 plugs into a socket in the groove between the two Rabaptin5 helices. The ARF-binding site of the GAT domain, which is not included in the construct used for crystallization, would be on the opposite side and located in the helix–loop–helix motif ~35 Å from the Rabaptin5-binding site (Zhu *et al*, 2003). The predicted ubiquitin-binding site (Shiba *et al*, 2004), however, overlaps with the Rabaptin5-binding area. No steric inhibition is observed in the symmetric potential GAT-binding site that would require major conformational changes for a second GAT–Rabaptin5 interaction to occur. An

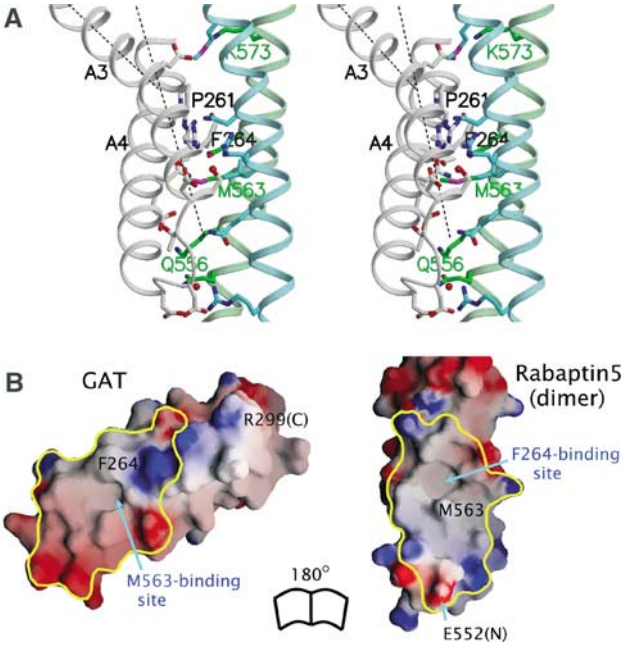

Figure 2 GAT–Rabaptin5 interaction. (**A**) Stereo view of the interface. Helix backbones are shown in a ribbon representation and colored as white, cyan, and green for GAT and the two Rabaptin5 monomers, respectively. Side chains of residues directly involved in the interface are shown in stick models and colored in blue (for nitrogen atoms), red (oxygen), and magenta (sulfur), or according to their backbone colors (carbon). Helices α_3 and α_4 of GAT are labeled as A3 and A4 (Zhu *et al*, 2003). The kink of helix α_3 is depicted by the axes of the two portions of the helix (black dash lines). (**B**) Molecular surface models of the GAT three-helix bundle (left) and N-terminal part of Rabaptin5$^{551-661}$ dimer (right). The color scheme is the same as Figure 1C. The interface regions, based on a calculation of buried SAS, are enclosed with yellow lines. Selected residues and (N- or C-) termini are labeled.

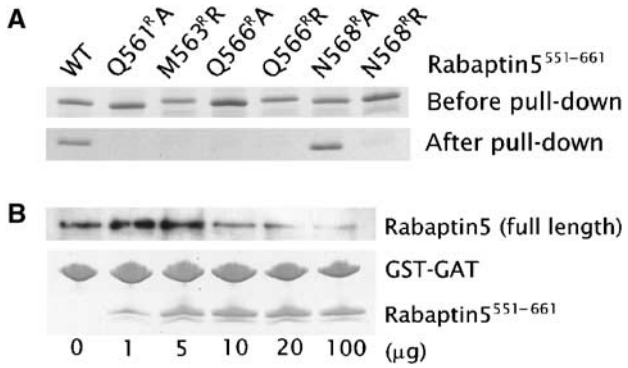

Figure 3 Binding affinity between Rabaptin5 fragment and GGA1 GAT domain. (**A**) GST-mediated pull-down assay. Purified recombinant GST-GGA1$^{141-326}$ is immobilized to GSH resin. Rabaptin5$^{551-661}$ variants from cell lysate (i.e. samples labeled as 'before pull-down') were pulled down by the GAT fusion protein and visualized with CBB stain (labeled as 'after pull-down'). (**B**) Competition of Rabaptin5$^{551-661}$ with full-length Rabaptin5 for GGA1 GAT. GST-GGA1$^{141-326}$ (10 μg) were preincubated with GSH-Sepharose beads and cell lysate containing full-length Rabaptin5 in the presence of different concentrations of Rabaptin5$^{551-661}$ (0–100 μg) to a final volume of 400 μl. The material bound to the beads was subjected to SDS–PAGE and CBB stain (for GST-GGA1$^{141-326}$ and Rabaptin5$^{551-661}$) or anti-Rabaptin5 Western blot (for full-length Rabaptin5). The experiment was repeated multiple times and was reproducible.

electrostatic potential change induced by the first GAT binding may provide an explanation for the affinity reduction in the symmetric binding site.

Binding assay on the GAT–Rabaptin5 interaction

Results from our previous mutagenesis studies on GGA1 GAT (Zhai *et al*, 2003) are consistent with the notion that the complex observed in the current crystal structure also exists in solution. The reduction of binding affinity to Rabaptin5 by any one of the point mutations P261E (i.e. Pro261 to Glu substitution), F264R, R265E, L277R, N284S, or D285R in GGA1 GAT (Zhai *et al*, 2003) can be explained based on the current complex structure: P261E introduces an acidic residue that interferes with Glu572^{R}, F264R disrupts a hydrophobic interaction, R265E increases the negative charge of GAT in the vicinity of Glu572^{R}, L277R interferes with Arg554^{R} and/or destabilizes hydrophobic interaction, N284S causes a loss of one critical hydrogen bond with Gln566^{R}, and D285R introduces a repulsive interaction with Lys559^{R} (Figure 2A and Supplementary Figure S2). Meanwhile, our GAT surface mutations not part of the structurally observed Rabaptin5-binding site show no effect on the binding (Zhai *et al*, 2003), suggesting that the GAT domain uses only one surface patch to interact specifically with Rabaptin5.

The current complex structure further allows us to test key surface residues from both monomers of the Rabaptin5$^{551-661}$ dimer through mutagenesis studies by making point mutations Q561^{R}A, M563^{R}R, Q566^{R}A, Q566^{R}R, N568^{R}A, and N568^{R}R in the Rabaptin5$^{551-661}$ parental construct. In the pull-down experiments, GGA1$^{141-326}$ (i.e. full-length GAT domain) was fused to glutathione *S*-transferase (GST), immobilized to resin beads, and incubated with the cell lysate containing individually expressed Rabaptin5$^{551-661}$ variants. The bound Rabaptin5$^{551-661}$ variants were further analyzed with SDS–PAGE. Alanine or arginine replacements at the selected positions of Rabaptin5$^{551-661}$ diminished the binding to GAT (Figure 3A), indicating that important components for Rabaptin5–GAT interactions seen in the complex structure are also operative in solution. To address the biological relevance of this interaction further, we employed a competition assay to determine if the full-length GAT domain–full-length Rabaptin5 interaction can be disrupted by the presence of the Rabaptin5$^{551-661}$ fragment (Figure 3B). Full-length Rabaptin5 was expressed in mammalian cells, and the cell lysate was pulled down with GST-GGA1$^{141-326}$ in the presence of varied concentrations of Rabaptin5$^{551-661}$. As the Rabaptin5$^{551-661}$ concentration increased, the binding of full-length Rabaptin5 to GAT diminished. This result suggests that *in vivo* Rabaptin5–GAT binding uses the same interface that is observed in the crystal structure.

Four-helix bundle of Rabaptin5

In the crystal structure, two Rabaptin5$^{551-661}$ homodimers from neighboring asymmetric units form a 190-Å-long tetramer related by the crystallographic two-fold symmetry. A single homo-four-helix bundle constitutes the entire tetramer interaction and possesses a pseudo-222-point symmetry (Figure 4A). Each helix of the bundle is about 50 residues long (i.e. residues 590–640) and is antiparallel to its nearest neighbors. Hydrophobic residues are packed in the core of the bundle. Charged and polar residues form extensive salt-bridge and hydrogen bonds on the surface. The buried SAS between the two symmetric dimers is 8300 Å^2, with 67%

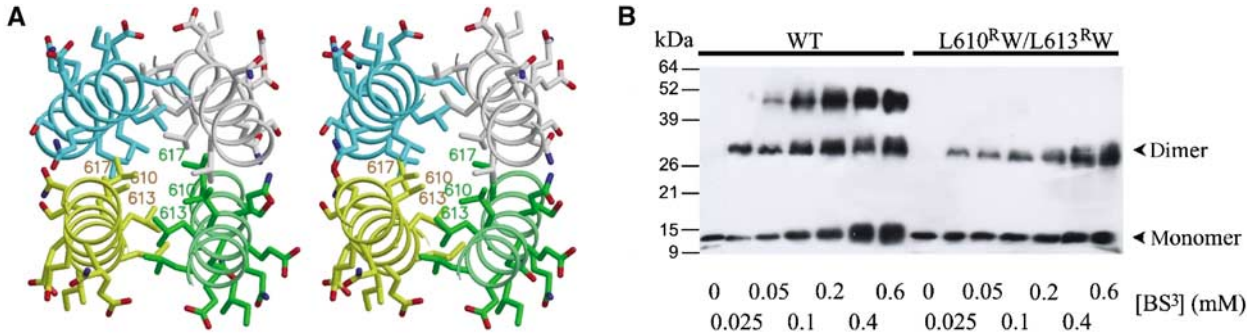

Figure 4 Rabaptin5 tetramerization. (**A**) Stereo view of the central section of the four-helix bundle of Rabaptin5$^{551-661}$. Backbones of the four helices are shown in ribbon representation and colored in yellow, green, cyan, and white, respectively. Side chains are shown in stick models and their carbon atoms are colored corresponding to their respective backbones. Other atoms are colored as in Figure 2A. Selected residues from the hydrophobic core are labeled. The yellow and white molecules belong to one parallel dimer, as do the cyan and green molecules, whereas the two dimers are antiparallel to each other. (**B**) Chemical crosslink. Tubes containing equal amounts of His_6-Rabaptin5$^{551-661}$ WT (left) or L610^{R}W/L613^{R}W mutant (right) were incubated with varied concentrations of BS^3 (0–0.6 mM) for 30 min at 22°C. The final crosslinked products were then subjected to 12% homogenous SDS–PAGE and analyzed with anti-His Western blot.

contributed by hydrophobic atoms. In comparison, the SAS buried between the two monomers in an isolated parallel Rabaptin5$^{551-661}$ homodimer is 2050 Å^2 and is mainly contributed by the N-terminal regions of the long helices.

The existence of this tetramerization structure in solution was detected with chemical crosslinking (Figure 4B), using a His-tagged recombinant protein sample directly purified from the soluble fraction of *E. coli* cell lysate. It showed that a significant fraction of Rabaptin5$^{551-661}$ can be crosslinked in forms of a molecular weight range higher than a dimer. This result was reproducible in a 300-fold range of protein concentration (data not shown), indicating that the oligomerization is not an artifact of high protein concentration. Furthermore, we constructed a Rabaptin5$^{551-661}$ variant of a double mutation L610^{R}W/L613^{R}W, which presumably disrupts the tetramer formation (see Figure 4A). Repeating the chemical crosslinking experiment with this Rabaptin5 mutant essentially eliminated the trimer/tetramer species but retained the dimer in the crosslinking product (Figure 4B). This result further supports that the crystallographically observed Rabaptin5 tetramer exists in solution. In addition, this L610^{R}W/L613^{R}W double mutant retained full GAT-binding ability as the wild type in a GST-mediated pull-down assay (data not shown), suggesting that the GAT-binding ability of Rabaptin5 is structurally independent of its tetramerization.

Discussion

GGA adaptors function in the vesicle transport pathway between TGN and endosomes in concert with an array of protein partners. Among them, Rabaptin5 binds with all three isoforms of human GGAs. Two Rabaptin5-binding sites have been identified on the GGA proteins (Mattera *et al*, 2003) (Supplementary Figure S3). One is located in the GAE domain of GGA1–3 (Hirst *et al*, 2000; Mattera *et al*, 2003). A crystal structure of GGA3 GAE in complex with a peptide of Rabaptin5$^{435-447}$ has been reported (Miller *et al*, 2003). This interaction occurs between an extended peptide of Rabaptin5 containing a sequence motif of FxxΦ (where Φ stands for a hydrophobic amino-acid residue) and the surface depression formed along the edges of two β-sheets present in the GAE domain. The second binding site occurs in the GAT domain of GGA1 and GGA2, but not in GGA3. Here, we demonstrate that this second Rabaptin5–GGA interaction is between the three-helix bundle of GGA GAT domain and a Rabaptin5$^{551-661}$ parallel coiled-coil homodimer. This GAT-binding region of Rabaptin5$^{551-661}$ is locally symmetrical; however, only one GAT domain is found to interact with the dimer in the current crystal structure (Figure 1B). Such an interaction may also occur *in vivo* for the following reasons. First, if two GAT domains could bind simultaneously to the Rabaptin5 dimer in a symmetrical way while both also attach to the membrane, it would require the two-fold axis of Rabaptin5 dimer to be more or less perpendicular to the membrane. Such a scenario is unlikely because the GAT-binding site is located in the middle of the elongated Rabaptin5 molecule. Second, the surfaces of both GGA1$^{210-302}$ and Rabaptin5$^{551-661}$ structures are highly negatively charged (Figure 1C) except for the binding interface (Figure 2B) where hydrophobic interaction contributes significantly. Therefore, electrostatic repulsion may prevent two GAT domains binding simultaneously to the Rabaptin5 dimer.

Although Rabaptin5 interacts equally well with the GAE domains from all three isoforms of human GGAs (Hirst *et al*, 2000; Mattera *et al*, 2003), it shows different binding affinities toward their GAT domains (Mattera *et al*, 2003; Zhai *et al*, 2003), that is, preferring the GAT domain of GGA1 and GGA2 over GGA3. The functional consequence of this difference is unclear at present. Among the residues of GGA1 GAT domain that directly interact with Rabaptin5$^{551-661}$, only residues 261 (Pro/Arg in GGA1 and GGA3, respectively), 265 (Arg/Lys), 284 (Asn/Ser), and 288 (Thr/Ser) are different between GGA1 and GGA3. Residue 261 is located at the kink position of helix α_3, which appears critical to the Rabaptin5 binding (Figure 2A). Its importance is supported by the deleterious effect of the P261E mutant (Zhai *et al*, 2003). Nevertheless, the GGA3-like P261R mutant interacts well with Rabaptin5, arguing that Pro261 may not be essential for the Rabaptin5-binding preference of GGA1. The two conserved mutations between GGA1 and GGA3, R265K and T288S, are expected to maintain similar interactions with the ligand; thus, they are unlikely to be the structural determinants causing the difference in preference. A more serious change is the N284S

substitution that results in the loss of one hydrogen bond with $Gln566^R$ and has been shown to diminish Rabaptin5 binding (Zhai *et al*, 2003). Moreover, it is interesting to see that a reversed mutant, S283N, can instill a significant Rabaptin5-binding ability in GGA3 (Zhai *et al*, 2003; Mattera *et al*, 2004). Furthermore, nonconserved residues that do not directly interact with Rabaptin5 may also influence the binding ability through subtle environmental changes (Mattera *et al*, 2004). For example, the region of sequence difference N-terminal to the 'kink' region of helix α_3, which does not directly contact Rabaptin5, may result in a local conformational change in the 'kink' region on the complex interface and subsequently disturb a salt-bridge bond between $Lys573^R$ and the position cognate to Glu257 of GGA1. In addition, the current crystal structure is consistent with the observation that Rabaptin5 does not interact with the GAT domain from TOM1 or TOM1-L1 (Mattera *et al*, 2004), since 11 out of 14 GGA1 residues that interact with Rabaptin5 in the current structure differ from those in TOM1 (Dell'Angelica *et al*, 2000). Interestingly, the same 'Rabaptin5-binding' region in the GAT domain from either GGA1 or GGA3, but not GGA2, is shown to bind with ubiquitin (Shiba *et al*, 2004). This interaction appears to be strengthened by ARF binding in the presence of N-terminal VHS domain of GGA, although structural modeling suggests that a ubiquitin monomer and ARF would bind to distinct structural motifs in the GAT domain that are over 30 Å away from each other. Similar ubiquitin binding has also been observed in the GAT domain of human TOM1 despite its relatively low sequence homology with GGAs (e.g. lower than that between GGA1 and GGA2). It appears that Rabaptin5 and ubiquitin would compete for the same binding site on the GAT domain three-helix bundle region, particularly the surface hydrophobic patch formed by helices α_3 and α_4 (Mattera *et al*, 2004; Shiba *et al*, 2004). Such a potential interference between the two interactions could form an additional layer of regulation in vesicle trafficking, that is, Rabaptin5–GAT interaction could be regulated by ubiquitin binding, or *vice versa*.

While there has been evidence suggesting that purified Rabaptin5 exists in solution as high-molecular-weight oligomers, the complexes are often interpreted as dimers (Vitale *et al*, 1998). Besides the GAT–$(Rabaptin5)_2$ interaction, to our surprise, our crystal structure reveals an unexpected four-helix bundle mediated homotetramerization of Rabaptin5. The interactions between the helices appear to be also stable in solution (Figure 4B). The $Rabaptin5^{551–661}$ dimer dimerization buries more than 8000 $Å^2$ SAS, and two-thirds of the buried SAS are from hydrophobic atoms. At present, we could not rule out the possibility that the tetramerization is an artifact of the recombinant protein fragment. For example, in full-length Rabaptin5, intramolecular interactions could replace the structurally observed tetramer interactions. Nevertheless, the extensive and complementary tetramer interface seen in the crystal structure favors an alternative interpretation. Although we have not determined the affinity for the tetramerization, structural comparison strongly suggests that the strength of the dimer–dimer interaction between $Rabaptin5^{551–661}$ is significantly higher than that of the GGA1 GAT–$Rabaptin5^{551–661}$ interaction. Unless drastically reorganized, an isolated $Rabaptin5^{551–661}$ dimer from the current structure would expose a large hydrophobic surface to solvent. Thus, a permanent tetramerization appears a way to stabilize this portion of the Rabaptin5 protein in solution (Nooren and Thornton, 2003). Since the surface of the four-helix bundle is dominated by negative charges, it seems unlikely that this Rabaptin5 fragment would form higher orders of homo-oligomers in solution once tetramerized. Because regions of Rabaptin5 on both sides of the GAT-binding domain also form homodimers (Vitale *et al*, 1998), the detailed dimerization scheme in the Rabaptin5 tetramer could be topologically complicated. A similar antiparallel tetramerization of two parallel dimers was proposed for another trafficking accessory protein, the Rab5 activator Rin2 (Saito *et al*, 2002), although it is not known whether the two cases of tetramerization are the same because of lack of detailed structural information on Rin2. The GAT-binding and tetramer-forming region of Rabaptin5 is highly conserved in evolution, with a better than 90% sequence identity in this region in general among species (in current GenBank). Compared with human Rabaptin5, the chicken Rabaptin5 has the lowest homology, being 84% identical and 91% conserved in this region (Figure 5). Nevertheless, in a modeling test, the current crystal structure can accommodate the chicken Rabaptin5 sequence without significant conformational adjustment (data not shown). In addition, the human Rabaptin5 homolog, Rabaptin5β (Gournier *et al*, 1998), is conserved in the four-helix bundle region but contains a deletion in the GAT-binding region compared to Rabaptin5 (Figure 5). It suggests that the four-helix bundle and the GAT-binding dimer region of Rabaptin5 are modular structural motifs, each bearing a distinct function. The coiled-coil four-helix bundle may hold multiple functions. For example, it could provide mechanical support and scaffold for other protein domains and/or bind specifically to some yet to be recognized partners.

Because Rabaptin5 plays important roles in early endosome fusion (Stenmark *et al*, 1995), it is hypothesized that the GGA–Rabaptin5 interaction enables fusion of TGN-derived vesicles with endosomes (Mattera *et al*, 2003), allowing the unloading of cargos from the TGN to endosomal system (Puertollano *et al*, 2003). Rabaptin5 interfering with the ARF–GGA–clathrin binding through steric and/or electrostatic mechanism may mediate this function. Currently available complex crystal structures allow us to assemble a model of the ARF–GAT–$Rabaptin5^{551–661}$ interaction with high confidence in its geometry (Figure 6). In this model, two GGA1 GAT domains independently bind to the opposite two ends of the $Rabaptin5^{551–661}$ tetramer of the current structure, retaining the 1:2 GAT (monomer) to Rabaptin5 (monomer) ratio. One ARF molecule interacts with each of the two GAT domains, assuming that ARF and Rabaptin5 simultaneously bind to the GAT domain (thus the GGA protein) (Zhai *et al*, 2003). Should such a complex exist *in vivo*, it could provide a linkage between two ARF molecules 200 Å apart.

Among the proteins of the current discussion, both GGA and Rabaptin5 are multidomain proteins, which dynamically interact with an array of partners in vesicular transport. With regard to the divalent interaction between GGA and Rabaptin5, it is interesting that GAT–Rabaptin5 interaction has a stoichiometry of 1:2 but the GAE–Rabaptin5 interaction has a 1:1 ratio (Supplementary Figure S3). Possibly, this would free up one extended peptide containing the FxxΦ motif from the Rabaptin5 dimer not bound to GAE to interact

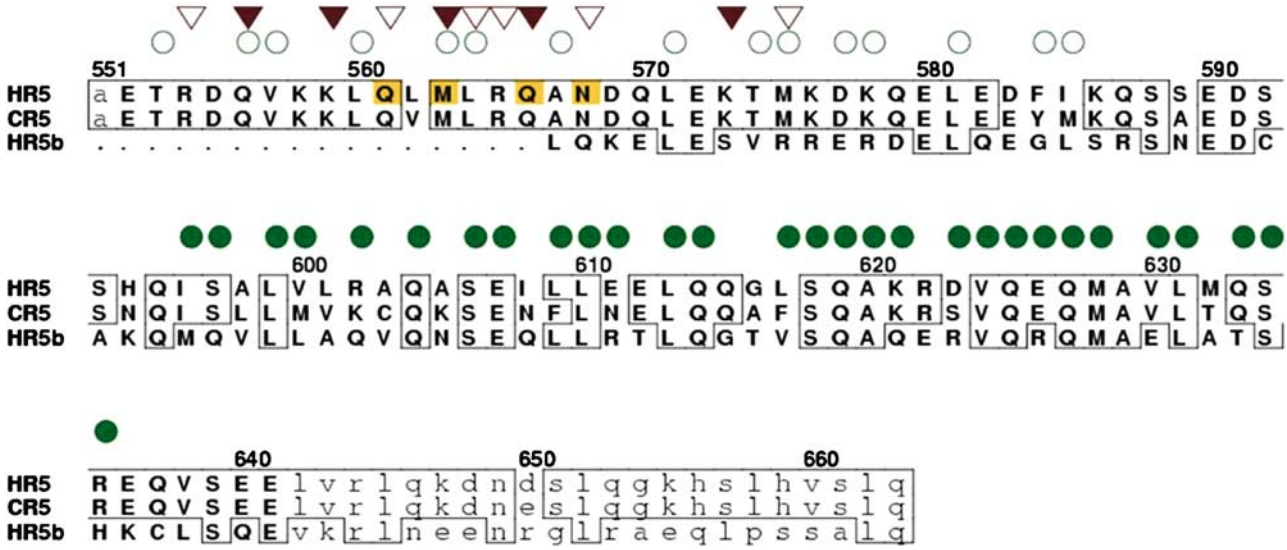

Figure 5 Sequence alignment of Rabaptin5 homolog proteins in the 'GAT-binding' region. The order from top to bottom is human Rabaptin5 (HR5, residues 551–663), chicken Rabaptin5 (CR5, residues 549–661, GenBank ID BAA21785), and human Rabaptin5β (HR5b, residues 287–383, GenBank ID RNU34932). The region of residues visible in the GAT–Rabaptin5 complex crystal is represented with capital letters, and mobile residues are in lowercase letters. HR5 residue numbers are labeled above the sequence. Residues identical to that of HR5 are boxed. Positions involved in the GAT binding from the two monomers of the Rabaptin5 dimer are marked with open and filled triangles, respectively. Positions involved in the N-terminal dimerization and C-terminal tetramerization (4 Å cutoff) are marked with open and filled circles, respectively. Residues of HR5 subjected to mutagenesis studies are highlighted.

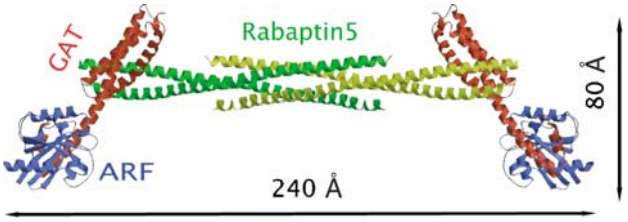

Figure 6 Ribbon diagram of a hypothetical ARF–GAT–(Rabaptin5)$_4$–GAT–ARF complex. The ARF molecule and ARF–GAT interaction are modeled according to the crystal structure of ARF–GAT peptide complex (PDB file 1J2J). The GAT domain is copied from the crystal structure of GGA1 GAT domain (1OXZ). The GAT–Rabaptin5 interaction and Rabaptin5 tetramer are based on the current crystal structure. Since the two ARF-binding sites are independent of each other, in solution an alterative arrangement is also possible, that is, the right side GAT–ARF complex could flip 180° about the dyad axis of the yellow Rabaptin5 dimer.

with another protein, and thereby expand the Rabaptin5 interacting network. Furthermore, the GAT and GAE domains interacting with one Rabaptin5 molecule may come from different GGA molecules. With the tetramerization, Rabaptin5 potentially assumes an even greater role in network formation. For example, its Rab5-binding motifs at the C-termini of the four monomers could reach the endosome membrane and regulate the tethering and fusion process.

Materials and methods

Protein expression and purification

Fusion constructs of GST-GGA1$^{210–302}$ (i.e. the three-helix bundle region of the GGA1 GAT domain) and GST-GGA1$^{141–326}$ (i.e. the full-length GAT domain of GGA1) were inserted into pGEX6P1 and pGEX2T (Amersham-Biosciences), respectively, as described previously (Zhai *et al*, 2003). Each was expressed as soluble recombinant protein in *E. coli* B21 (DE3) cells and purified with GSH-Sepharose 4B affinity chromatography (Amersham-Biosciences). The GGA1$^{210–302}$ protein was separated from gel-immobilized GST after cleavage with the PreScission protease (Amersham-Biosciences) and was further purified with Resource-Q anion-exchange chromatography (Amersham-Biosciences). The protein sample was concentrated to 20 mg ml^{-1} (based on $\varepsilon_{280} = 2.7$ AU mM^{-1}, estimated using the program *VectorNTI* from InforMax Inc.). The GST-GGA1$^{141–326}$ fusion protein was left intact for the pull-down assay, purified as previously described (Zhai *et al*, 2003), and concentrated to 12 mg ml^{-1} ($\varepsilon_{280} = 1.0$ AU mM^{-1}, *VectorNTI*). Se-Met-substituted GGA1$^{210–302}$ was prepared by using the same construct as the native protein. It was expressed in *E. coli* B834 (DE3) pLysS cells (Novagen) grown in minimal media plus 40 mg l^{-1} Se-Met (Sigma). The construct encoding Rabaptin5$^{551–661}$ was subcloned into pET11a (Novagen), expressed as inclusion bodies, refolded using the rapid dilution method (Lin *et al*, 1989) with dithiothreitol (DTT) as the reducing agent, and purified as described before (Zhai *et al*, 2003). For crystallization and pull-down assay, the Rabaptin5 protein was concentrated to 8 mg ml^{-1} (based on the Bradford protein assays, Bio-Rad Laboratories) in 10 mM HCl–Tris (pH 8.0) and stored on ice. Mass spectroscopic and N-terminal analyses showed that this sample contained two species of residues 551–642 and 551–648, respectively, both of which had an extra N-terminal methionine derived from the starting codon. The ratio of the two species (~1:1) remained unchanged during a 2-month period according to SDS–PAGE analyses. For the crosslink experiment, a His$_6$-Rabaptin5$^{551–661}$ fusion construct and its L610^{R}W/L613^{R}W double mutant were inserted separately into the pET15b vector (Novagen) and expressed in *E. coli* BL21 (DE3) cells. The cell culture of each variant was lysed using the CelLytic bacterial lysis buffer (Sigma) containing protease inhibitors and DNAse (Roche), incubated for 15 min at 22°C, and clarified by centrifugation for 15 min at 60 000 *g*. The supernatant was then applied to His-select affinity resin (Sigma), washed, and eluted. The sample was dialyzed against 1 × phosphate-buffered saline (PBS, pH 7.5), and its concentration was estimated by comparison to known concentrations of bovine serum albumin since the 280-nm extinction coefficient of the Rabaptin5 sample is extremely low to nonexistent.

Crystallization and data collection

The initial crystallization condition of the GGA1$^{210–302}$–Rabaptin5$^{551–661}$ complex was obtained using Hampton Research crystallization

screening kits, by varying the concentration ratio of the two protein components and cross-seeding with a tetragonal form of $GGA1^{210–302}$ crystal (G Zhu and XC Zhang, unpublished data). Crystals of good diffraction quality were obtained under the following condition: protein samples of $GGA1^{210–302}$ (20 mg ml^{-1}) and $Rabaptin5^{551–661}$ (8 mg ml^{-1}) were first mixed 1:2 (v/v), then this sample was mixed 2:1 (v/v) with the reservoir solution containing 1.1 M $(NH_4)_2SO_4$, 0.1 M Tris (pH 9.0), and 0.1% (v/v) β-mercaptoethanol. The complex crystals were grown at 20°C using the hanging drop method. Native crystals grew to $0.8 \times 0.4 \times 0.3$ mm from a 4.5 µl drop over a 500 µl reservoir in 10 days, and Se-Met derivative crystals to $0.5 \times 0.2 \times 0.15$ mm under similar conditions. The crystals were soaked in a mixture of saturated Li_2SO_4 and the reservoir solution (4:1) for cryoprotection before transference to a 100 K nitrogen gas stream for data collection.

X-ray diffraction data from the crystal of native $GGA1^{210–302}$–$Rabaptin5^{551–661}$ complex were collected up to 2.4 Å resolution from an in-house MAR345 image plate (Mar Research Inc.) using a single crystal. For the Se-Met derivative crystal, a three-wavelength multiple anomalous dispersion (MAD) dataset was collected to 2.8 Å resolution at the F2 beam line of the Cornell High Energy Synchrotron Source (CHESS) using a Quantum-210 CCD detector system. Data were processed with the *HKL* program suite (Otwinowski and Minor, 1997). Both the native and Se-Met derivative crystals were shown to be hemihedrally twinned (Yeates, 1997), with twinning fractions of 0.41 and 0.13, respectively. The data were detwinned correspondingly as the last step of data processing.

Structural determination and refinement

Most of the crystallographic calculations, including detwinning the data, were performed with the program suite *CNS* (Brunger *et al*, 1998). The MAD dataset yielded four selenium sites, which correspond to the four Met residues positioned at 231, 233, 249, and 259 previously found in one GGA1 GAT domain (Zhu *et al*, 2003). The MAD phases of the Se-Met derivative yielded an initial experimental electron density map at 2.8 Å resolution. The phases were further improved and extended to 2.4 Å resolution by density modification and switching to the native dataset. The resulting density map was interpretable for the most part. The crystal form was found to belong to the $P3_221$ space group, with a 5.4 Å^3 Da^{-1} V_M, assuming one GAT and two Rabaptin5 fragments per asu. Manual model building was carried out with the program *Turbo-Frodo* (Roussel and Cambillau, 1989), with the three-helix bundle model from our previously reported GGA1 GAT crystal structure (PDB file 1OXZ) as a partial initial model. Structural refinement consisted of several rounds of torsion angle simulated-annealing and restrained individual *B*-factor refinements, using a maximum likelihood target function against native data up to the highest resolution available. The final $R_{working}$ was 0.235 for the detwinned dataset, and 0.181 for the twinned dataset using a corresponding target function in *CNS*. SAS was calculated using a 1.4 Å probe radius.

GST-mediated pull-down assay for studying GAT–Rabaptin5 interaction

To verify Rabaptin5 residues involved in GAT binding, point mutations were introduced into the $Rabaptin5^{551–661}$ parental construct and expressed in *E. coli*. The soluble form of variant protein was used directly from cell lysate without further purification. GST-$GGA1^{141–326}$ was used for its stronger binding with $Rabaptin5^{551–661}$ than that of the GST-$GGA1^{210–302}$ fusion construct. In the pull-down experiment, recombinant fusion protein GST-$GGA1^{141–326}$ (30 µg) was incubated for 30 min at 22°C with 40 µl of a 50% slurry of GSH-Sepharose 4B in a final volume of 500 µl binding buffer containing 1 × PBS (pH 7.4), 0.2% (v/v) Triton X-100, and 0.2% (v/v) β-mercaptoethanol, supplemented with protease inhibitor cocktail. Beads containing immobilized GST fusion protein were washed three times by resuspension in 1 ml of 1 × PBS and centrifugation (3 min, 2000 *g*). Washed beads were incubated for 2 h at 22°C with equal volumes of cell lysate containing $Rabaptin5^{551–661}$ variants (~100 µg total protein) in 1 ml binding buffer, washed three times with 1 ml of binding buffer, and resuspended in 30 µl of 2 × SDS sample buffer. The sample was subjected to 20% SDS–PAGE analysis and visualized by Coomassie brilliant blue (CBB) stain.

Competition assay testing GAT–full-length Rabaptin5 interaction

A pcDNA3.1 expression vector containing the full-length human Rabaptin5 was transfected into HEK293 cells using the Lipofectamin 2000 transfection kit (Invitrogen). The transfected cells were grown in a T-25 culture flask for 36 h, resuspended in buffer A containing 1 × PBS, 1 mM EDTA, 1 mM $MgCl_2$, 1 mM DTT, 1% (v/v) NP-40 detergent, and protease inhibitor cocktail, and then lysed by repeated ejection through a 21-gauge needle. The lysate was clarified by 10 000 *g* centrifugation for 10 min at 4°C followed by 120 000 *g* for 1 h at 4°C. An aliquot of clarified supernatant (200 µl containing ~100 µg total protein) was incubated in buffer A containing 20 µg of GST-$GGA1^{141–326}$ (prebound to 40 µl of 50% slurry GSH-Sepharose 4B beads) in the presence of varied concentrations of $Rabaptin5^{551–661}$ (400 µl final volume) for 2 h at 22°C with gentle shaking. The beads were washed three times with 500 µl of buffer A, 25 µl of 2 × SDS sample buffer was added, and then the sample was subjected to 10% SDS–PAGE and blotted onto PVDF membrane (Millipore Co.). The blot was incubated sequentially with monoclonal mouse anti-Rabaptin5 antibody (BD Biosciences), which does not crossreact with the $Rabaptin5^{551–661}$ fragment, then peroxidase-conjugated anti-mouse IgG (Sigma) and detected on film using Renaissance Chemiluminescence Reagent plus (Amersham-Biosciences). The presence of $Rabaptin5^{551–661}$ in the complex was confirmed by CBB stain.

Chemical crosslink of $Rabaptin5^{551–661}$

To test for oligomer formation, recombinant protein of His_6-$Rabaptin5^{551–661}$ purified from the soluble fraction of *E. coli* cell lysate was crosslinked using bis-(sulfosuccinimidyl suberate) (BS^3, Pierce) reagent following the manufacturer's recommended protocol. Aliquots of His_6-$Rabaptin5^{551–661}$ (4 µg ml^{-1}) in 1 × PBS (pH 7.5) were added to each tube and incubated with varying concentrations of BS^3 (0–0.6 mM) for 30 min at 22°C. The reaction was quenched by adding 60 µl of 1 M Tris–HCl (pH 7.5) to each tube and incubated for 15 min at 22°C. For final analysis, the samples were applied to a 12% SDS mini-gel (Bio-Rad), transferred to PVDF membrane using a semidry transfer cell (Bio-Rad), and immunolabeled with mouse anti-His antibodies (Amersham-Biosciences). The anti-His-positive proteins were detected on film after a 4-min exposure following treatment of the membrane with ECL™ Western Blotting reagents (Amersham-Biosciences). To test for concentration dependence of crosslink oligomer formation, the same experiment was repeated with varied protein concentrations (0.7–220 µg ml^{-1}), analyzed with SDS–PAGE, and stained with anti-His Western blot or CBB. To confirm the importance of the hydrophobic core in tetramer formation in solution, we introduced a double mutant, $L610^RW/L613^RW$, into the His_6-$Rabaptin5^{551–661}$ construct and repeated the chemical crosslink experiment against that of the wild type.

Structural data deposition

Coordinates and the experimental structural factors of the $GGA1^{210–302}$–$Rabaptin5^{551–661}$ complex crystal structure have been deposited in PDB under code 1X79.

Supplementary data

Supplementary data are available at *The EMBO Journal* Online.

Acknowledgements

We thank W Radosevich for excellent technical assistance, Dr Q Hao and the staff of the F2 beam line at the CHESS synchrotron facility for help in data collection, and Dr T Mather for critical reading of the manuscript. We are grateful to Dr M Robinson (University of Cambridge) for providing the cDNA of human GGAs, and Dr G Grenningloh (University of Lausanne) for the Rabaptin5 cDNA. The Molecular Biology Resource Facility of University of Oklahoma Health Sciences Center performed DNA oligomer synthesis, total amino-acid analysis, and mass spectroscopic analysis. This work was supported in part by a grant from Oklahoma Center for the Advancement of Science and Technology to XZ, an NIH grant (AG-18933) and Alzheimer's Association Pioneer Award to JT, and an NSF CAREER award to GL.

References

Boman AL (2001) GGA proteins: new players in the sorting game. *J Cell Sci* **114:** 3413–3418

Boman AL, Zhang C, Zhu X, Kahn RA (2000) A family of ADP-ribosylation factor effectors that can alter membrane transport through the *trans*-Golgi. *Mol Biol Cell* **11:** 1241–1255

Brunger AT, Adams PD, Clore GM, DeLano WL, Gros P, Grosse-Kunstleve RW, Jiang JS, Kuszewski J, Nilges M, Pannu NS, Read RJ, Rice LM, Simonson T, Warren GL (1998) Crystallography & NMR system: a new software suite for macromolecular structure determination. *Acta Crystallogr D* **54:** 905–921

Collins BM, Watson PJ, Owen DJ (2003) The structure of the GGA1-GAT domain reveals the molecular basis for ARF binding and membrane association of GGAs. *Dev Cell* **4:** 321–332

Dell'Angelica EC, Puertollano R, Mullins C, Aguilar RC, Vargas JD, Hartnell LM, Bonifacino JS (2000) GGAs: a family of ADP ribosylation factor-binding proteins related to adaptors and associated with the Golgi complex. *J Cell Biol* **149:** 81–94

Deneka M, Neeft M, Popa I, van Oort M, Sprong H, Oorschot V, Klumperman J, Schu P, van der Sluijs P (2003) Rabaptin-5alpha/rabaptin-4 serves as a linker between rab4 and gamma(1)-adaptin in membrane recycling from endosomes. *EMBO J* **22:** 2645–2657

Gournier H, Stenmark H, Rybin V, Lippe R, Zerial M (1998) Two distinct effectors of the small GTPase Rab5 cooperate in endocytic membrane fusion. *EMBO J* **17:** 1930–1940

Hirst J, Lui WW, Bright NA, Totty N, Seaman MN, Robinson MS (2000) A family of proteins with gamma-adaptin and VHS domains that facilitate trafficking between the *trans*-Golgi network and the vacuole/lysosome. *J Cell Biol* **149:** 67–80

Kirchhausen T (2000) Clathrin. *Annu Rev Biochem* **69:** 699–727

Korobko EV, Kiselev SL, Korobko IV (2002) Multiple Rabaptin-5-like transcripts. *Gene* **292:** 191–197

Lin XL, Wong RN, Tang J (1989) Synthesis, purification, and active site mutagenesis of recombinant porcine pepsinogen. *J Biol Chem* **264:** 4482–4489

Lupas A (1996) Coiled coils: new structures and new functions. *Trends Biochem Sci* **21:** 375–382

Mattera R, Arighi CN, Lodge R, Zerial M, Bonifacino JS (2003) Divalent interaction of the GGAs with the Rabaptin-5–Rabex-5 complex. *EMBO J* **22:** 78–88

Mattera R, Puertollano R, Smith WJ, Bonifacino JS (2004) The trihelical bundle subdomain of the GGA proteins interacts with multiple partners through overlapping but distinct sites. *J Biol Chem* **279:** 31409–31418

Miller GJ, Mattera R, Bonifacino JS, Hurley JH (2003) Recognition of accessory protein motifs by the gamma-adaptin ear domain of GGA3. *Nat Struct Biol* **10:** 599–606

Moss J, Vaughan M (1998) Molecules in the ARF orbit. *J Biol Chem* **273:** 21431–21434

Nooren IM, Thornton JM (2003) Diversity of protein–protein interactions. *EMBO J* **22:** 3486–3492

Otwinowski Z, Minor W (1997) Processing of X-ray diffraction data collected in oscillation mode. *Methods Enzymol* **276:** 307–326

Poussu A, Lohi O, Lehto VP (2000) Vear, a novel Golgi-associated protein with VHS and gamma-adaptin 'ear' domains. *J Biol Chem* **275:** 7176–7183

Puertollano R, Aguilar RC, Gorshkova I, Crouch RJ, Bonifacino JS (2001) Sorting of mannose 6-phosphate receptors mediated by the GGAs. *Science* **292:** 1712–1716

Puertollano R, Bonifacino JS (2004) Interactions of GGA3 with the ubiquitin sorting machinery. *Nat Cell Biol* **6:** 244–251

Puertollano R, van der Wel NN, Greene LE, Eisenberg E, Peters PJ, Bonifacino JS (2003) Morphology and dynamics of clathrin/GGA1-coated carriers budding from the *trans*-Golgi network. *Mol Biol Cell* **14:** 1545–1557

Roussel A, Cambillau C (1989) TURBO-FRODO. In *Sillicon Graphics Geometry Partners Directory*, pp 77–79. Mountain View, CA: Silicon Graphics

Saito K, Murai J, Kajiho H, Kontani K, Kurosu H, Katada T (2002) A novel binding protein composed of homophilic tetramer exhibits unique properties for the small GTPase Rab5. *J Biol Chem* **277:** 3412–3418

Scott PM, Bilodeau PS, Zhdankina O, Winistorfer SC, Hauglund MJ, Allaman MM, Kearney WR, Robertson AD, Boman AL, Piper RC (2004) GGA proteins bind ubiquitin to facilitate sorting at the *trans*-Golgi network. *Nat Cell Biol* **6:** 252–259

Shiba T, Kawasaki M, Takatsu H, Nogi T, Matsugaki N, Igarashi N, Suzuki M, Kato R, Nakayama K, Wakatsuki S (2003) Molecular mechanism of membrane recruitment of GGA by ARF in lysosomal protein transport. *Nat Struct Biol* **10:** 386–393

Shiba Y, Katoh Y, Shiba T, Yoshino K, Takatsu H, Kobayashi H, Shin HW, Wakatsuki S, Nakayama K (2004) GAT (GGA and Tom1) domain responsible for ubiquitin binding and ubiquitination. *J Biol Chem* **279:** 7105–7111

Shiba Y, Takatsu H, Shin HW, Nakayama K (2002) gamma-Adaptin interacts directly with Rabaptin-5 through its ear domain. *J Biochem (Tokyo)* **131:** 327–336

Stenmark H, Vitale G, Ullrich O, Zerial M (1995) Rabaptin-5 is a direct effector of the small GTPase Rab5 in endocytic membrane fusion. *Cell* **83:** 423–432

Suer S, Misra S, Saidi LF, Hurley JH (2003) Structure of the GAT domain of human GGA1: a syntaxin amino-terminal domain fold in an endosomal trafficking adaptor. *Proc Natl Acad Sci USA* **100:** 4451–4456

Takatsu H, Yoshino K, Nakayama K (2000) Adaptor gamma ear homology domain conserved in gamma-adaptin and GGA proteins that interact with gamma-synergin. *Biochem Biophys Res Commun* **271:** 719–725

Takatsu H, Yoshino K, Toda K, Nakayama K (2002) GGA proteins associate with Golgi membranes through interaction between their GGAH domains and ADP-ribosylation factors. *Biochem J* **365:** 369–378

Vitale G, Rybin V, Christoforidis S, Thornqvist P, McCaffrey M, Stenmark H, Zerial M (1998) Distinct Rab-binding domains mediate the interaction of Rabaptin-5 with GTP-bound Rab4 and Rab5. *EMBO J* **17:** 1941–1951

Yeates TO (ed) (1997) *Detecting and Overcoming Crystal Twinning*. New York: Academic Press

Zhai P, He X, Liu J, Wakeham N, Zhu G, Li G, Tang J, Zhang XC (2003) The interaction of the human GGA1 GAT domain with Rabaptin-5 is mediated by residues on its three-helix bundle. *Biochemistry* **42:** 13901–13908

Zhu G, Zhai P, He X, Terzyan S, Zhang R, Joachimiak A, Tang J, Zhang XC (2003) Crystal structure of the human GGA1 GAT domain. *Biochemistry* **42:** 6392–6399